Biochimica et Biophysica Acta, 777 (1984) 183–193
Elsevier

BBA 72255

TIME-RESOLVED FLUORESCENCE EMISSION SPECTRA OF LABELED PHOSPHOLIPID VESICLES, AS OBSERVED USING MULTI-FREQUENCY PHASE-MODULATION FLUOROMETRY

JOSEPH R. LAKOWICZ [a], HENRYK CHEREK [a,*], GABOR LACZKO [a,**] and ENRICO GRATTON [b]

[a] *University of Maryland School of Medicine, Department of Biological Chemistry 660 West Redwood Street, Baltimore, MD 21201 and* [b] *University of Illinois at Urbana-Champaign, Department of Physics, Urbana, IL 61801 (U.S.A.)*

(Received April 16th, 1984)

Key words: Phospholipid vesicle; Fluorescent problem; Time-resolved fluorescence emission; Phase-modulation fluorimetry

Multi-frequency phase-modulation fluorometry was used to determine the time-resolved spectral parameters of two different fluorescent probes, 6-palmitoyl-2-[(2-trimethylammonium)ethyl]methylamino]naphthalene chloride (Patman) and 2-*p*-toluidinyl-6-naphthalenesulfonic acid (TNS) in lipid vesicles. The frequency-domain measurements permitted calculation of time-resolved emission spectra, the time-resolved decays of the emission center of gravity and of the emission spectral width. Nanosecond spectral relaxation was found using both probes, and these rates increased with temperature. The detailed time-domain information available using our method indicated that spectral relaxation of TNS is mainly a continuous process, whereas relaxation of Patman shows the characteristic features of a stepwise relaxation. Our results indicate that complex excited-state processes can be quantified using frequency-domain fluorometry.

Introduction

It is widely recognized that the emission spectra of fluorophores are sensitive to the polarity of their surrounding environment. For many fluorophores, this sensitivity is a combination of the specific chemical interactions between the fluorophore and the solvent and of the general effects of solvent polarity, such as are described by the Lippert equation [1–3]. Consequently, the emission spectral properties of fluorophores can reveal detailed information concerning the interactions between fluorophores and solvents. Furthermore, the absorption of light by a fluorophore provides an essentially instantaneous perturbation of the fluorophore-solvent interactions. Hence, the time-dependent spectra parameters reveal the time-course of these rather complex intermolecular interactions. For instance, time-resolved decays of fluorescence intensity have been utilized in detailed studies of the dynamic interactions of fluorophore and solvents [4–6] and biological macromolecules [7,8]. Also, such measurements have been used to distinguish between stepwise and continuous relaxation processes [5,9] and to detect the subnanosecond formation of partially relaxed fluorophores [4].

The technique of phase-modulation fluorometry has been less used to analyze excited-state processes. This technique has been used to detect excited-state processes [10,11], to detect the reversibility of an excited-state reaction [12] and to

* On leave from Nicholas Copernicus, University of Torun, Poland.

** On leave from the Josef Atilla University, Szeged, Hungary.

Abbreviations: Patman, 6-palmitoyl-2-[(2-trimethylammonium)ethyl]methylamino]naphthalene chloride; TNS, 2-*p*-toluidinyl-6-naphthalenesulfonic acid; DOPC and DPPC, dioleoyl and dipalmitoyl-L-α-phosphatidylcholine.

partially resolve the emission spectra of excited states [13,14]. Because only two or three modulation frequencies have been available, the information available from phase-modulation fluorometry has been less detailed than that obtained from time-resolved measurements. However, with the construction of a continuously variable frequency phase fluorometer, it is now possible to evaluate the potential of frequency-domain fluorescence spectroscopy. Recent developments allow the modulation frequency to be varied from 1 to 140 MHz [15], and more recently to 200 MHz (Lakowicz and Maliwal [29]). We used the former instrument to examine phospholipid vesicles labeled with the fluorescent probes Patman or TNS. These probes, when bound to lipid vesicles, display substantial time-dependent spectral shifts [11,16,17]. Spectral relaxation of TNS was reported to be well-described by the continuous model of Bakhshiev [16,18], whereas the currently available information on Patman indicated a stepwise relaxation process [17]. These studies [17] also proved that the spectral shifts are due to time-dependent processes, and not to heterogeneity in the emitting population of fluorophores. Hence, by examination of these probes, we could determine the usefulness of frequency-domain fluorometry for both the determination of time-resolved emission spectra and for a detailed analysis of complex time-dependent processes.

Theory

Models for time-dependent spectral shifts

A complete theoretical description of time-dependent shifts, based upon known molecular interactions between the fluorophore and solvent, is not currently available. Such a description would require a complete quantitative understanding of the general polarity and specific chemical effects of solvents upon the spectral properties of the fluorophore. We will consider two phenomenological models for spectral relaxation, one being a continuous model, and the second a two-state model. The spectral properties of these extreme cases are illustrated in Fig. 1. In both models, it is assumed that following a δ-pulse excitation, the emission spectra shift from an initially excited state (0) to an equilibrium state (∞). The center of gravity of the emission spectra of these limiting states are given by $\bar{\nu}_0$ and $\bar{\nu}_\infty$, respectively.

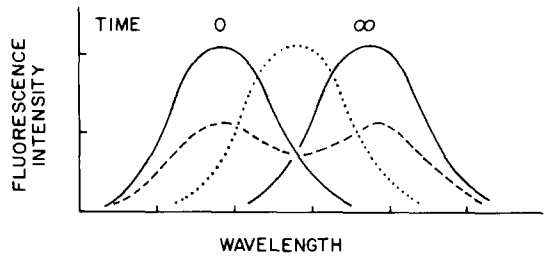

Fig. 1. Schematic description of the continuous and two-state models of solvent relaxation. The expected instantaneous spectra at intermediate times are shown for the two-state (- - - - - -) and the continuous (· · · · · ·) relaxation models. Also shown are the spectra expected at $t = 0$ and $t =$ infinity (∞).

Assume that the emission spectra could be observed at any desired instant. At longer times, the spectra will be shifted to longer wavelengths. For continuous relaxation, the normalized emission spectrum is assumed to slide to longer wavelength, without any change in the emission spectral distribution. Hence, irrespective of the time chosen to observe the emission, a constant spectral shape is expected (...) and the time-dependent spectral widths are expected to be independent of time. Overtly different results are expected for the two-state model. In this case, the initially excited and the equilibrium states are assumed to be distinct species, each with a characteristic emission spectrum. As the reaction proceeds, the emission from the initially excited state decays, followed by the appearance of a new emission at longer wavelengths (Fig. 1). At intermediate times, one would observe emission from both states (- - -). In practice, the observation of separate emission maxima for both states is unlikely because of the spectral width of most emission spectra and the limited solvent sensitivity of most fluorophores. Distinct emission maxima are observable for excited state chemical reactions such as deprotonation or excimer formation [12,14]. Furthermore, for a two-state model, the emission at each wavelength can be described by two exponential decay constants. These decay constants are independent of emission wavelengths, whereas the fractional intensity of each component is wavelength dependent [9,22]. In the case of continuous relaxation, the decay at

each wavelength is nonexponential and the apparent decay times are dependent upon the emission wavelength [1,5,8].

These two models provide a useful framework within which to consider spectral relaxation. Consider the instantaneous emission spectra at times comparable to the spectral decay rate. For continuous relaxation, one expects these time-resolved spectra to have the same spectral shape. Hence, if one measures the time-resolved spectral width, this should be independent of time. Contrasting results are expected for the two-state model. In this case, the spectral width is expected to be larger at intermediate times because of the contribution of both the initially excited and the equilibrium excited states.

Impulse response functions from frequency-domain fluorescence

The time-resolved spectral parameters (emission spectra, center of gravity, and spectral widths) can be calculated from the impulse response functions, if these are known at each emission wavelength. Typically, these decay laws are found using time-resolved measurements of the intensity decays, followed by deconvolution to account for the finite width of the excitation pulse. In our case, the impulse response functions were determined using measurements of the phase ($\phi_\omega(\lambda)$) and modulation ($m_\omega(\lambda)$) of the emission, over a range of emission wavelengths (λ) and modulation frequencies (ω). Typically, we used about ten emission wavelengths and ten modulation frequencies for each wavelength, ranging from 2.5 to 140 MHz. These data were fit, using the method of nonlinear least squares [19,20] to the function:

$$I(\lambda,t) = \sum_{i=1}^{3} \alpha_i(\lambda) e^{-t/\tau_i} \tag{1}$$

In principle, the decay at each emission wavelength, λ is probably more complex than a sum of exponentials. This was particularly evident from the decays time from two-exponential fits. Then, the decay times were dependent upon the emission wavelength. This indicates that the relaxation process is more complex than a one-step event. Furthermore, for a continuous relaxation process [5,9], the decay times are probably distinct at each emission wavelength. In practice, with three decay times, we found that it was not necessary to allow both $\alpha_i(\lambda)$ and the decay times to vary with emission wavelength. We found that impulse response functions which allowed wavelength-dependent preexponential factors and wavelength-independent decay times (Eqn. 1) provided a very good representation of measured data. In several cases, we performed a less restricted analysis in which the τ_i values were determined independently at each wavelength, i.e., $\tau_i(\lambda)$. The goodness of fit was not substantially improved using this model with more variable parameters. This fact is illustrated by the values of χ^2_R listed in Tables I and II. Essentially identical values were obtained using Eqn. 1 or a less restrictive procedure in which the decay times were allowed to vary at each wavelength. This indicates that Eqn. 1 provides a reasonable model. Importantly, the time-dependent parameters were not substantially different for wavelength-dependent or independent values of the decay times. This invariance indicates that our time-resolved results are independent of our use of Eqn. 1 to fit the frequency-domain data.

The values of the $\alpha_i(\lambda)$ and τ_i in Eqn. 1 were determined by minimizing the sum of the squared deviations between the measured ($\phi_\omega(\lambda)$ and $m_\omega(\lambda)$) and calculated values ($\phi_{c\omega}(\lambda)$ and $m_{c\omega}(\lambda)$). The chosen parameters were those which resulted in the minimum value of χ^2,

$$\chi^2 = \sum_{\omega,\lambda} \frac{1}{\sigma^2_{\phi\omega}} (\phi_\omega - \phi_{c\omega})^2 + \sum_{\omega,\lambda} \frac{1}{\sigma^2_{m\omega}} (m_\omega - m_{c\omega})^2 \tag{2}$$

In this expression, $\sigma_{\phi\omega}$ and $\sigma_{m\omega}$ are the uncertainties in the measured phase and modulation values, respectively. We used the values given in Materials and Methods, which were found to be appropriate for our instrument and our experimental conditions.

The phase and modulation values for any assumed decay law can be calculated from the sine and cosine transforms of the decay law [21,22]. Let

$$N_\omega(\lambda) = \frac{\int_0^\infty I(\lambda,t)\sin \omega t \, dt}{\int_0^\infty I(\lambda,t) dt} \tag{3}$$

$$D_\omega(\lambda) = \frac{\int_0^\infty I(\lambda,t)\cos \omega t \, dt}{\int_0^\infty I(\lambda,t) dt} \tag{4}$$

Then, substitution of Eqn. 1 yields:

$$N_\omega(\lambda)J(\lambda) = \sum_i \frac{\alpha_i(\lambda)\omega\tau_i^2}{1+\omega^2\tau_i^2} \tag{5}$$

$$D_\omega(\lambda)J(\lambda) = \sum_i \frac{\alpha_i(\lambda)\tau_i}{1+\omega^2\tau_i^2} \tag{6}$$

where

$$J(\lambda) = \sum_i \alpha_i(\lambda)\tau_i \tag{7}$$

The expected values of the phase and modulation are obtained from:

$$\phi_{c\omega}(\lambda) = \arctan(N_\omega(\lambda)/D_\omega(\lambda)) \tag{8}$$

$$m_{c\omega}(\lambda) = \left(N_\omega(\lambda)^2 + D_\omega(\lambda)^2\right)^{1/2} \tag{9}$$

The goodness of fit can be judged from the value of reduced χ^2

$$\chi_R^2 = \chi^2/\nu \tag{10}$$

where ν is the number of degrees of freedom. In our case, ν is typically near 177 (100 phase angles and 100 modulation values minus 23 floating parameters for a three-exponential decay law). In the decay law, there are three values for τ_i and 20 values for $\alpha_i(\lambda)$. At each wavelength, there are two independent values of $\alpha_i(\lambda)$, since $\Sigma_i\alpha_i(\lambda) =$ constant.

Time-resolved emission spectra

In our presentation of the impulse response functions ($I(\lambda,t)$) we chose to normalize the preexponential factors α_i such that $\Sigma|\alpha_i| = 2$. In this way, equal and opposite preexponential factors, such as are expected for excited-state processes, would be evident from values of $\alpha_i(\lambda)$ ranging from -1 to $+1$ (Tables I and II). Calculation of the time-resolved emission spectra requires that the impulse-response functions be normalized [16]. Specifically, the total intensity at each wavelength must be normalized to the steady-state intensity at this same wavelength ($F(\lambda)$). Let

$$H(\lambda) = \frac{F(\lambda)}{\int_0^\infty I(\lambda,t)\mathrm{d}t} \tag{11}$$

$$= \frac{F(\lambda)}{\alpha_1(\lambda)\tau_1 + \alpha_2(\lambda)\tau_1 + \alpha_3(\lambda)\tau_3} \tag{12}$$

Then, the appropriately normalized functions are given by

$$I'(\lambda,t) = H(\lambda)I(\lambda,t) \tag{13}$$

$$= \sum_i \alpha_i'(\lambda)e^{-t/\tau_i} \tag{14}$$

where $\alpha_i'(\lambda) = H(\lambda)\alpha_i(\lambda)$. For any desired time ($t_i$), the time-resolved emission spectrum is obtained by plotting the values $I'(\lambda,t_i)$.

Time-resolved emission center of gravity

The time-dependent spectral shifts can be characterized by the time-dependent center of gravity, in wavenumbers (cm^{-1} or kK), which is proportional to the average energy of the emission. The center of gravity of the emission is defined by:

$$\bar{\nu}_{cg}(t) = \frac{\int_0^\infty I'(\bar{\nu},t)\bar{\nu}\mathrm{d}\bar{\nu}}{\int_0^\infty I'(\bar{\nu},t)\mathrm{d}\bar{\nu}} \tag{15}$$

where $I'(\bar{\nu},t)$ represent the number of photons per wavenumber interval. Our data were collected at equally spaced wavelength intervals [23], and using an emission monochromator with a constant bandpass in nanometers [24]. For these conditions, the center of gravity in kK ($= 10^3$ cm^{-1}) is given by:

$$\bar{\nu}_{cg}(t) = 10000\frac{\sum_\lambda I'(\lambda,t)\lambda^{-1}}{\sum_\lambda I'(\lambda,t)} \tag{16}$$

Spectral width of the emission spectrum

The time-dependent spectral width $\Delta\bar{\nu}(t)$ (cm^{-1}) can reveal whether the spectral relaxation is best described by continuous or a stepwise process [9,22]. We chose to characterize this parameter using:

$$\Delta\bar{\nu}(t) = \frac{\int_0^\infty (\bar{\nu} - \bar{\nu}_{cg}(t))^2 I'(\bar{\nu},t)\mathrm{d}\bar{\nu}}{\int_0^\infty I'(\bar{\nu},\mathrm{d})\mathrm{d}\bar{\nu}} \tag{17}$$

This value is comparable to the standard deviation of the fluorescence intensity. For measurement using equally spaced wavelengths and constant resolution in nanometers, $\Delta\bar{\nu}(t)$ in kK is given by:

$$\Delta\bar{\nu}(t) = \frac{\sum_{\lambda}\left(10000/\lambda - \bar{\nu}_{cg}(t)\right)^2 I'(\lambda,t)}{\sum_{\lambda} I'(\lambda,t)} \qquad (18)$$

Materials and Methods

Phase and modulation measurements were performed on the instrument described previously [15]. All measurements were performed relative to a scattering reference of Ludox in water. In contrast to the phase fluorometers with a Debye-Sears modulator [25], this instrument appears to be mostly free of artifacts upon comparison of scattered and fluorescence intensity. The excitation was at 351 nm, using an argon ion laser. The emission was observed through a Jarrell-Ash 1/4 meter monochromator and an emission bandpass of 6.6 nm. For the Patman-labeled vesicles, a Corning 3-75 filter was used on the emission. No emission filter was used for the TNS-labeled vesicles. The excitation was polarized near 35° from the vertical, and the emission was observed without a polarizer. Any effects due to rotational diffusion are likely to be minor. The background signal from unlabeled vesicles under identical conditions was 2% or less of the signal resulting from the labeled samples, at all emission wavelengths. The weighting factors for the least-square fit were $\sigma_{\phi\omega} = 0.21 + 0.84 \log_{10} f$ and $\sigma_{\phi m} = 0.0084 + 0.0087 \log_{10} f$, where f is the modulation frequency in MHz. These values are 3-fold larger than those used previously [26]. About ten wavelengths were used for most measurements. At each wavelength, the phase angle and modulation were measured using approximately ten frequencies. Patman-labeled and TNS-labeled vesicles were prepared as described previously [17,23].

Results

Patman-labeled phospholipid vesicles

The steady-state emission spectra of Patman-labeled vesicles are shown in Fig. 2. Above the transition temperature of the DPPC vesicles, the emission spectrum of Patman shifts dramatically to longer wavelengths. For the DOPC vesicles, which are above their transition temperature even at 6 °C, the emission spectrum is broad even at low temperature. At higher temperature, the emission spectrum becomes more narrow and shifts to longer wavelengths. From earlier measurements, we know that these spectral shifts are due to time-dependent processes on the nanosecond timescale [10,17,27]. Frequency-dependent phase and modulation data for Patman-labeled DPPC vesicles are shown in Fig. 3. It is not practical to display the data at all emission wavelengths. Instead, we chose to show the data obtained at three emission wavelengths, located on the blue, center and red sides of the emission. These data are characteristic of an excited-state reaction [27]. That is, the phase angles increase and the modulation decreases with increasing emission wavelength. Furthermore, the data are unambiguous in demonstrating the occurrence of a time-dependent process which occurs subsequent to excitation. The apparent phase and modulation lifetimes at each

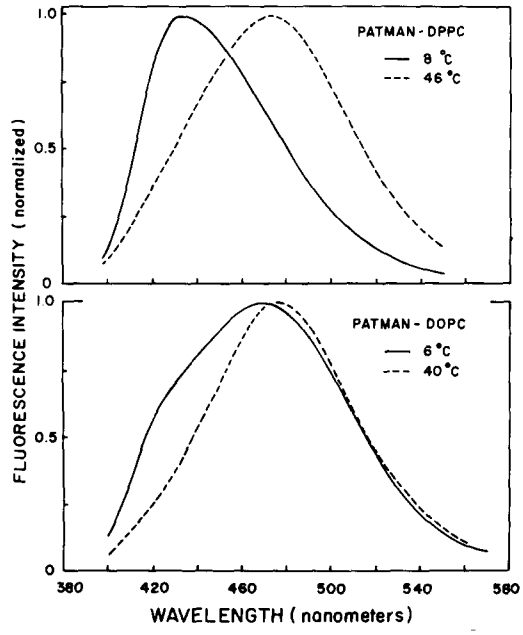

Fig. 2. Steady-state emission spectra of Patman-labeled phospholipid vesicles. Top, DPPC vesicles at 8 (———) and 46 °C (- - - - - -). Bottom, DOPC vesicles at 6 (———) and 40 °C (- - - - - -).

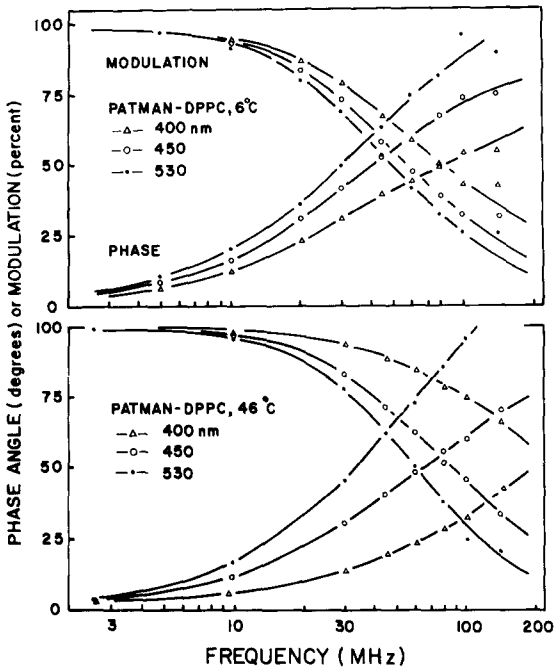

Fig. 3. Frequency-dependent phase and modulation values for Patman-labeled DPPC vesicles. Top, 6 °C; bottom, 46 °C. For both temperatures, data are shown for 400 (△), 450 (○) and 530 (●) nm.

frequency increase with the modulation frequency (data not shown), and the measured phase angles exceed 90°. This is not possible for a mixture of directly excited fluorophores [10,27]. It is interesting to compare the results for Patman – DPPC at low and high temperature (Fig. 3). At high temperature and on the blue side of the emission, the phase angles are shorter, and the modulation values higher, than observed at lower temperature. This distinction reflects the shortened decay time on the blue side of the spectrum due to faster relaxation at the higher temperature. At longer emission wavelengths, the data for higher temperature are more characteristic of an excited-state process, as is evident from the phase angles which exceed 90°.

The phase and modulation data were used to derive the wavelength-dependent impulse response functions, as described in Theory. Typical values for the Patman-labeled DPPC vesicles are summarized in Table I. The three decay times are similar at both 8 and 46°C. The main distinction

TABLE I

IMPULSE RESPONSE FUNCTION FOR PATMAN-LABELED DPPC VESICLES

At 8 °C, the value of χ^2_R, obtained using wavelength independent decay times, was 1.38. By comparison, the value of χ^2_R obtained using variable lifetimes at each emission wavelength was also 1.38. This is the average of the values obtained from 400 to 530 nm. At 46 °C, χ^2_R for the listed impulse response functions was 0.72. For the less restrictive fits, the average value of χ^2_R was 0.79.

8 °C			
(τ, ns)	(0.98 ns)	(3.74 ns)	(5.52 ns)
Wavelength	$\alpha_1(\lambda)$ [a]	$\alpha_2(\lambda)$	$\alpha_3(\lambda)$
400	1.15	0.60	0.25
410	0.87	0.74	0.39
430	0.21	1.02	0.77
450	−0.13	0.95	0.92
470	−0.40	0.73	0.87
490	−0.50	0.57	0.93
510	−0.61	0.33	1.06
530	−0.74	0.18	1.08
46 °C			
(τ, ns)	(0.95 ns)	(1.48 ns)	(3.94 ns)
Wavelength	$\alpha_1(\lambda)$	$\alpha_2(\lambda)$	$\alpha_3(\lambda)$
400	1.84	–	0.10
410	1.51	0.39	0.10
430	0.52	1.16	0.32
450	−0.56	0.91	0.53
470	−0.77	0.45	0.78
490	−0.85	0.14	1.01
510	−0.71	−0.20	1.09
530	−0.50	−0.42	1.07
550	−0.04	−0.90	1.06

[a] The sum of the absolute values of $\alpha_i(\lambda)$ are set to 2.0 at each wavelength.

between these results is the larger contribution of terms with negative preexponential factors at the higher temperature. Such terms are characteristics of emission which is formed by an excited-state process. At the longest emission wavelengths, these positive and negative terms are nearly equal in magnitude and opposite in sign. This is a characteristic of emission from the product of an excited-state process without substantial contribution from the emission due to the initially excited state [28]. Comparable results were found for the DOPC vesicles.

Time-resolved emission spectra of the Patman-labeled vesicles are shown in Figs. 4 and 5. To

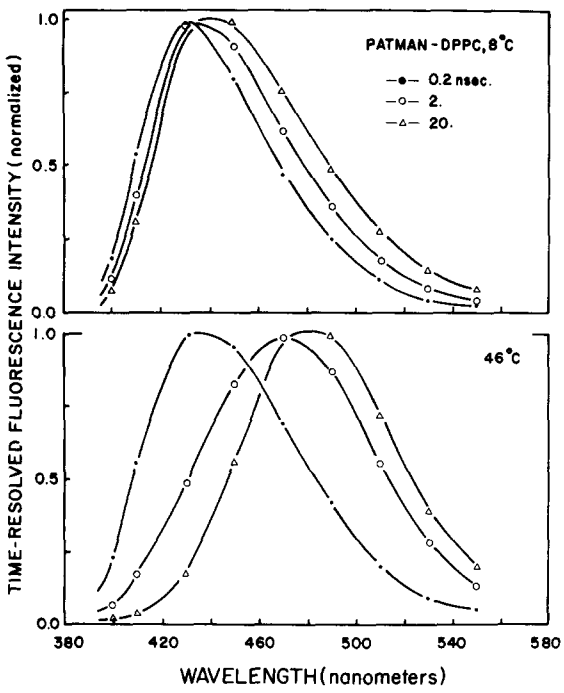

Fig. 4. Time-resolved emission spectra of Patman-labeled DPPC vesicles. Top, 8 °C; bottom, 46 °C. Time-resolved spectra are shown at 0.2 (●), 2 (○) and 20 ns (△).

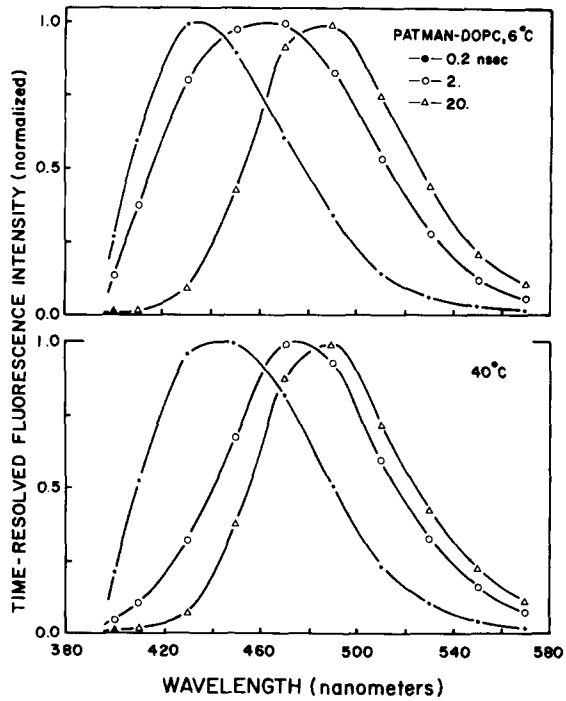

Fig. 5. Time-resolved emission spectra of Patman-labeled DOPC vesicles. Top, 6 °C; bottom, 40 °C. Time-resolved emission spectra are shown at 0.2 (●), 2 (○) and 20 ns (△).

facilitate the comparison of these spectra we chose to display, in each case, time-resolved spectra at 0.2, 2 and 20 ns. For DPPC, below its transition temperature, there is only a modest red shift at 20 ns, about 15 nm. At 46 °C, a dramatic spectral shift is seen to occur between 0.2 and 20 ns, about 50 nm. Also, at 2 ns the time-resolved emission spectrum of Patman appears wider than at 0.2 and 20 ns. This is consistent with a two-state model for spectra relaxation.

Time-resolved spectra for DOPC vesicles are shown in Fig. 5. In this case, a dramatically broadened spectrum is seen at 2 ns at 6 °C. The spectral widths are obviously more narrow at 0.2 and 20 ns, indicating that spectral relaxation has not proceeded substantially at 0.2 ns and that it is mostly complete at 20 ns. At higher temperature, the spectral relaxation appears to be more rapid. This is evident from the nearly relaxed spectrum seen at 2 ns at 40 °C.

A more quantitative measure of the rates of spectral relaxation can be obtained from the time-dependent decay of the center of gravity ($\bar{\nu}_{cg}(t)$). These results are summarized in Fig. 6. For DPPC, both the extent and rate of spectral relaxation are increased above the transition temperature. For the DOPC vesicles, a similar amount of energy (2.5 kK) is lost at low and high temperature, and the rate of decay is increased at the higher temperature. It appears that spectral relaxation is more rapid in DOPC than in DPPC vesicles. The relaxation times appear to be near 2 ns. If desirable, these time-dependent values of $\bar{\nu}_{cg}(t)$ could be used to calculate the decay law for the center of gravity. A preliminary examination of these data revealed that the decay is more complex than a single exponential.

We also examined the time-dependent changes in the spectral widths ($\Delta\bar{\nu}(t)$) (Fig. 7). In all cases, except for DPPC at 8 °C, there is a substantial increase in spectral width at intermediate times. The increased width is the result of contributions from the initially excited and the relaxed states to the emission spectrum. At higher temperature, this

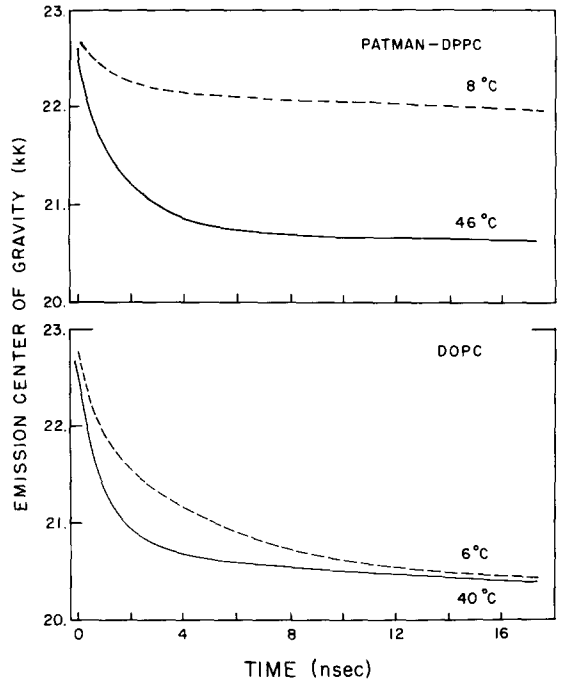

Fig. 6. Time-resolved emission center of gravity of Patman-labeled vesicles. Top, DPPC at 8 (- - - - - -) and 46 °C (———). Bottom, DOPC at 6 (- - - - - -) and 40 °C (———).

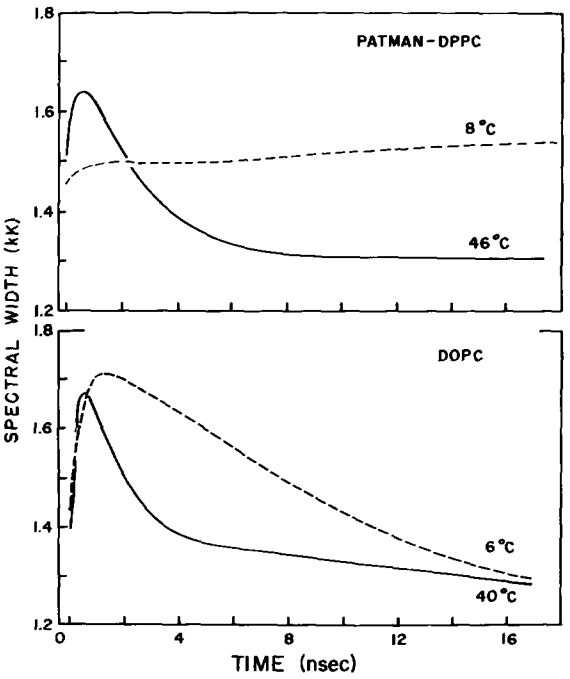

Fig. 7. Time-resolved spectral width of Patman-labeled vesicles. Top, DPPC at 8 (- - - - - -) and 46 °C (———). Bottom, DOPC at 6 (- - - - - -) and 40 °C (———).

increase in $\Delta\bar{\nu}(t)$ is of shorter duration, reflecting a more rapid decay to the equilibrium excited state. This transient increase in $\Delta\bar{\nu}(t)$ suggests that the spectral relaxation of Patman is best described by the two-state model.

TNS-labeled phospholipid vesicles

For comparative purposes, we also examined vesicles labeled with TNS. The temperature-dependent spectral shifts of TNS are substantially smaller than those observed for Patman (Fig. 8). The impulse-response functions at each emission wavelength were obtained from frequency-dependent phase and modulation data. These results were also again consistent with an excited-state reaction. This was evident from the negative preexponential factors in the impulse-response functions. Typical values for TNS bound to DPPC at 4 °C are listed in Table II.

Time-resolved emission spectra of TNS-labeled DOPC are shown in Fig. 9. Compared to the Patman-labeled vesicles (Fig. 6), the total spectral

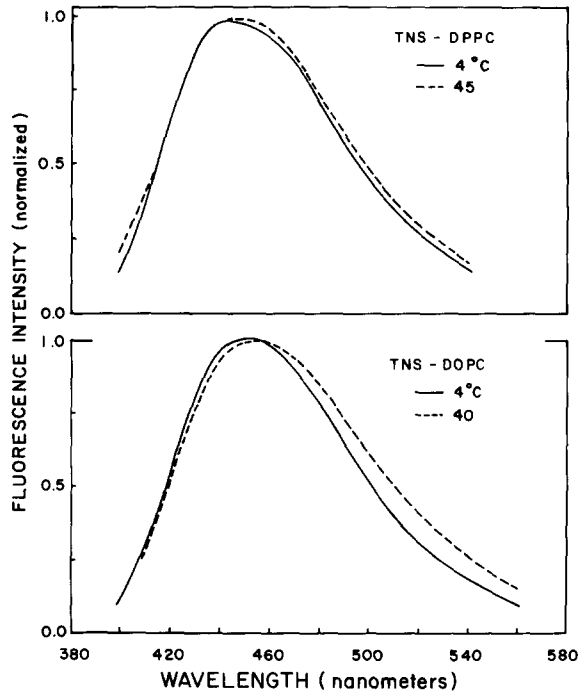

Fig. 8. Steady-state emission spectra of TNS-labeled vesicles. Top, DPPC at 4 (———) and 45 °C (- - - - - -). Bottom, DOPC at 4 (———) and 40 °C (- - - - - -).

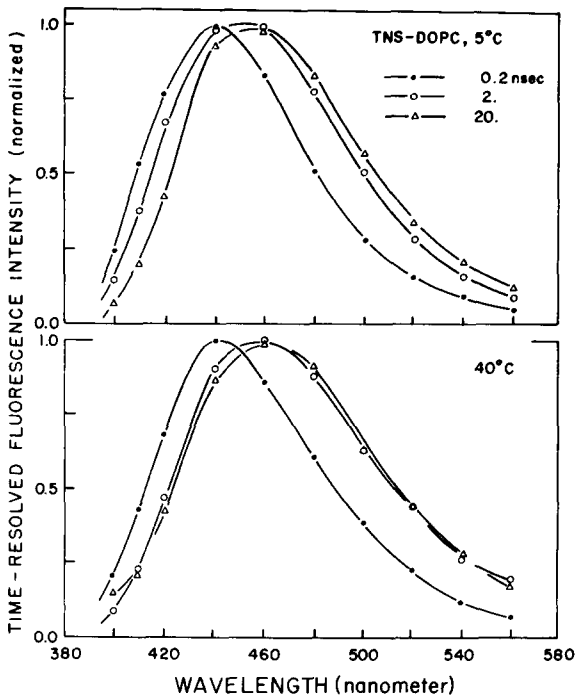

Fig. 9. Time-resolved emission spectra of TNS-labeled DOPC vesicles. Top, 5 °C; bottom, 40 °C. Time-resolved emission spectra are shown at 0.2 (●), 2 (○) and 20 (△) ns.

shifts are reduced. Higher temperatures result in faster relaxation, as may be seen by comparing the spectra at 2 ns at 5 and 40 °C. At 40 °C, spectral relaxation seems to be essentially complete at 2 ns. The time-dependent values of $\bar{\nu}_{cg}(t)$ are summarized in Fig. 10. In the case of DOPC, an increased rate of spectral decay is seen at higher temperature. For the DPPC vesicles, increased temperature has a smaller effect.

Finally, the time-resolved spectral widths of the TNS-labeled vesicles are summarized in Fig. 11. Once again, an increase in $\Delta\bar{\nu}(t)$ is seen at intermediate times near 2 ns. However, in contrast to the substantial increase in $\Delta\bar{\nu}(t)$ seen for Patman-labeled vesicles (Fig. 7), the $\Delta\bar{\nu}(t)$ values for TNS are rather constant (Fig. 11). It appears that the spectral relaxation of TNS can be approximately described by a continuous model. However, we caution that the apparent constancy of $\Delta\bar{\nu}(t)$ of TNS may be the result of the smaller shift which occurs upon relaxation, rather than a relaxation

TABLE II

IMPULSE RESPONSE FUNCTION FOR TNS-LABELED DPPC AT 4 °C

For the impulse response function shown, $\chi^2_R = 0.47$, For the less restrictive fit, with variable lifetimes at each wavelength, $\chi^2_R = 0.43$.

Wavelength (τ, ns)	$\alpha_1(\lambda)$ [a] (0.44)	$\alpha_2(\lambda)$ (2.67)	$\alpha_3(\lambda)$ (10.5)
400	0.74	0.84	0.43
410	0.32	1.00	0.68
420	−0.09	0.98	0.93
440	−0.35	0.66	0.99
460	−0.68	0.45	0.87
480	−0.85	0.35	0.80
500	−1.02	0.33	0.65
520	−0.99	0.27	0.77
540	−1.10	0.23	0.63

[a] $\Sigma_i|\alpha_i(\lambda)| = 2.0$.

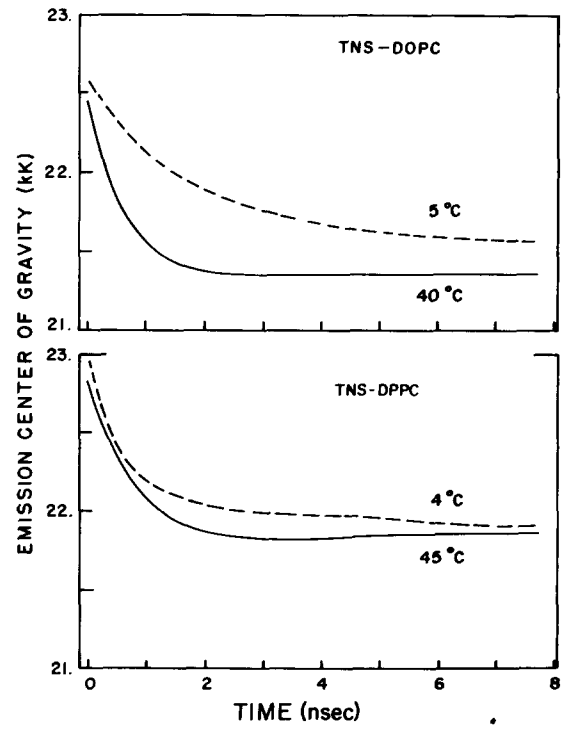

Fig. 10. Time-resolved center of gravity of TNS-labeled vesicles. Top, DOPC at 5 (- - - - - - -) and 40 °C (———). Bottom, DPPC at 4 (- - - - - -) and 45 °C (———).

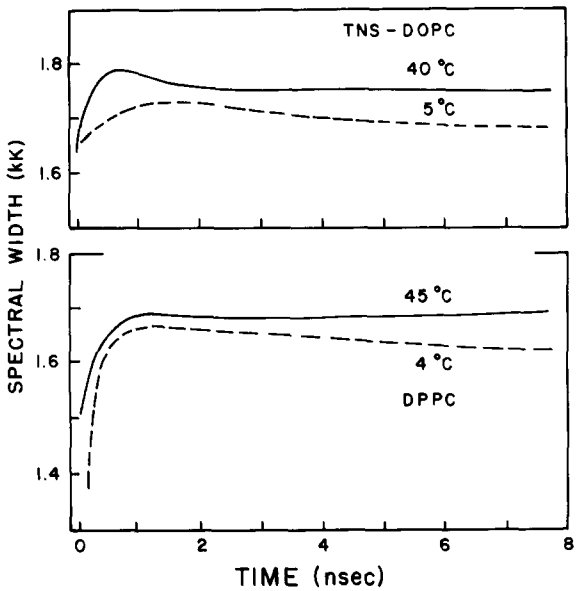

Fig. 11. Time-resolved spectral widths of TNS-labeled vesicles. Top, DOPC at 5 (- - - - -) and 40 °C (———). Bottom, DPPC at 4 (- - - - -) and 45 °C (———).

mechanism which is fundamentally different from that which occurs for Patman.

Discussion

It is interesting to speculate about molecular origin of the relaxation processes observed in the phospholipid vesicles. In solvents, spectral relaxation is generally the result of reorientation of the solvent molecules in response to the electronic distribution of the excited state. In vesicles, we found that the rate of relaxation was dependent upon the physical state of the vesicles. This fact, and the rather long relaxation times, suggest that the bulk water has a minimum effect on the relaxation process. We cannot rigorously exclude bound water as contributing to the relaxation. However, it seems likely that the observed spectral relaxation is the result of either a reorientation of the lipids around the excited state dipole of the fluorophores or a reorientation of the probe. Both processes are known to be dependent upon the physical state of the vesicles, and both processes could occur simultaneously. However, our information is not sufficiently detailed to permit identification of the molecular events which are responsible for spectral relaxation.

Our results represent the first detailed description of time-resolved emission spectra using frequency-domain fluorometry. As must be true for any new method, further studies are likely to yield a more detailed and quantitative description of spectral relaxation. In fact, we decided not to emphasize such analyses, but rather to emphasize the practical usefulness of frequency-domain fluorometry for such measurements. Several general observation can be made with confidence. The time-resolved spectral properties of fluorophores may be easily and reliably obtained from the frequency-domain measurements. The rates of spectral relaxation are in agreement with those estimated previously using the time-resolved method [11,16,23] and phase-sensitive detection of fluorescence [11] for TNS-labeled vesicles. Also, in the case of Patman, the results are in agreement with earlier studies in which the spectral relaxation was examined by phase-sensitive detection of fluorescence [17]. We confirmed that spectral shifts of Patman are due to time-dependent spectral shifts and not ground-state heterogeneity, and that the relaxation is not adequately described by a continuous relaxation model [17]. Importantly, the results appear to be sufficiently precise to reveal changes in the relaxation rates due to temperature, and due to differences in the nature of the relaxation process, that is continuous or stepwise.

It seems valuable to comment on the time required to obtain the frequency-domain measurements. In these initial experiments, the data were collected by manually changing the wavelengths and recording the values. Even so, all the necessary data at a single temperature could be obtained in about 2 h. If needed, this time could be reduced by automation. In conclusion, frequency-domain fluorometry can provide rapid and reliable quantitation of complex time-dependent processes.

Acknowledgements

The authors thank Dr. Badri Maliwal for assistance in preparation of the samples and analysis of the data. This study was supported by Grant PCM 80-41320, 81-06910 and 82-10878 to J.R.L., and PCM 79-18646 to E.G., all from the National Science Foundation.

References

1 Norporent, B.S. and Bakhshiev, N.G. (1960) Opt. Spectrosc. 8, 408–413
2 Perov, A.N. (1980) Opt. Spectrosc. 49, 371–374
3 Van Lippert, E. (1957) Z. Electrochem. 61, 962–975
4 Ware, W.R., Lee, S.K., Brant, C.J. and Chow, P.P. (1970) J. Chem. Phys. 54, 4729–4737
5 DeToma, R.P., Easter, J.H. and Brand, L. (1976) J. Am. Chem. Soc. 98, 5001–5007
6 Badea, M.G. and Brand, L. (1979) Methods Enzymol. 61, 378–425
7 Lakowicz, J.R. (1980) J. Biochem. Biophys. Methods 2, 91–119
8 Badea, M.G., DeToma, R.P. and Brand, L. (1978) Biophys. J. 24, 197–212
9 DeToma, R.P. and Brand, L. (1977) Chem. Phys. Lett. 47, 231–236
10 Lakowicz, J.R., Cherek, H. and Bevan, D.R. (1980) J. Biol. Chem. 255, 4403–4406
11 Lakowicz, J.R., Thompson, R.B. and Cherek, H. (1983) Biochim. Biophys. Acta 734, 295–308
12 Lakowicz, J.R. and Balter, A. (1982) Chem. Phys. Lett. 12, 117–121
13 Lakowicz, J.R. and Balter, A. (1982) Photochem. Photobiol. 36, 125–132
14 Lakowicz, J.R. and Balter, A. (1982) Biophys. Chem. 16, 117–132
15 Gratton, E. and Limkeman, M. (1983) Biophys. J. 44, 315–324
16 Easter, J.H., DeToma, R.P. and Brand, L. (1976) Biophys. J. 16, 571–583
17 Lakowicz, J.R., Bevan, D.R., Maliwal, B.P., Cherek, H. and Balter, A. (1983) Biochemistry 22, 5714–5722
18 Bakhshiev, N.G., Mazurenko, Yu.T. and Piterskaya, J.V. (1966) Opt. Spectrosc. 21, 307–309
19 Marquardt, D.W. (1963) J. Soc. Ind. Appl. Math. 11, 431–441
20 Lakowicz, J.R., Gratton, E., Laczko, G., Cherek, H. and Limkeman, M. (1984) Biophys. J. 46, 463–477
21 Weber, G. (1977) J. Chem. Phys. 66, 4081–4091
22 Lakowicz, J.R. (1983) Principles of Fluorescence Spectroscopy, Plenum Publishing Co., New York
23 Lakowicz, J.R. and Hogen, D. (1981) Biochemistry 20, 1366–1373
24 Meehuish, W.H. (1961) J. Phys. Chem. 65, 229–235
25 Lakowicz, J.R. and Cherek, H. (1981) J. Biochem. Biophys. Methods 5, 131–146
26 Gratton, E., Lakowicz, J.R., Maliwal, B., Cherek, H., Laczko, G. and Limkeman, M. (1984) Biophys. J. 46, 479–486
27 Lakowicz, J.R. and Balter, A. (1982) Biophys. Chem. 16, 99–115
28 Laws, J.R. and Brand, L. (1979) J. Phys. Chem. 83, 795–802
29 Lakowicz, J.R. and Maliwal, B.P. (1984) Biophys. Chem., in the press